Ultrasonic RF-based imaging for the purposes of characterizing the microstructure of solid tumors

Michael L. Oelze[1], James F. Zachary[2] and William D. O'Brien Jr.[1]

[1]Department of Electrical and Computer Engineering, [2]Department of Veterinary Pathology
University of Illinois at Urbana-Champaign

ABSTRACT

Eight retired breeder rats were acquired that had developed spontaneous mammary tumors. Tumors were diagnosed microscopically as mammary gland fibroadenomas. Two-dimensional gray-scale B-mode images of the tumors in the rats were constructed from backscattered echoes using an 8 MHz (90% bandwidth) single element ultrasonic transducer. From the gray-scale B-mode images, regions-of-interest (ROIs) were selected in the tumors and surrounding tissues. The power spectra of backscattered RF echoes gated from the ROIs were used to estimate the average scatterer diameters and concentrations. A unique estimation scheme was used to obtain the average scatterer diameters and concentrations. The average scatterer diameter was related to the slope of the best-fit line to the reduced measured power spectrum versus the frequency squared. The scatterer concentration was determined from the intercept of the best-fit line. The reduced measured power spectrum is the measured power spectrum minus 40 log of the frequency. Parametric B-mode images were constructed by converting ROI boxes into colored pixels. The color of the pixels was related to the estimated scatterer properties. The images showed a distinct difference between the tumor and surrounding healthy tissues. Scatterer sizes inside the tumor were on average 30% larger than scatterer sizes in surrounding normal tissues.

Keywords: Ultrasound, RF-based imaging, backscatter, tissue characterization, parametric imaging

I. INTRODUCTION

Conventional B-mode images of tissues using ultrasound are made from the backscattered RF signals. Processing of the backscattered RF signals in conventional B-mode images takes out the frequency-dependent information contained in the signals. The frequency dependence of the signals is hypothesized to contain information about the tissue microstructure.

Several models exist that relate frequency-dependent backscatter from tissues to the microstructure.[1,2] These models have been used to estimate average properties (size, shape and scatter strength) of tissue microstructures from backscattered RF signals for the purposes of detecting and classifying diseased tissues.[2,3] Enhanced (parametric) B-mode images have been constructed that incorporate scatterer property estimates.

Parametric images have been used to assess tissues.[3,4,5] Rapid classification of tissues through imaging techniques is medically significant to treatment of disease. The classification of disease through imaging of tissue microstructures offers a noninvasive diagnostic technique. Parametric ultrasound imaging has the ability to rapidly classify and diagnose diseased tissue. In this work a parametric imaging technique is explored and results are examined to determine the utility of the imaging technique for tissue classification.

II. THEORY

The scattering from soft tissues in this study are modeled by a 3-D spatial autocorrelation function

$$b_z(\Delta r) \tag{1}$$

Medical Imaging 2002: Ultrasonic Imaging and Signal Processing, Michael F. Insana, William F. Walker, Editors, Proceedings of SPIE Vol. 4687 (2002) © 2002 SPIE · 1605-7422/02/$15.00

where z is the relative impedance between the scattering particle and surrounding tissues. The 3-D spatial autocorrelation function describes the size, shape and distribution of particles by their impedance change with surrounding tissues. The theoretical power spectrum, which relates the frequency dependence of the backscattered RF signals to the scattering properties, is the Fourier transform of the 3-D spatial autocorrelation function

$$W_{theor}(\mathbf{K}) = \frac{V}{(2\pi)^6}\int_{-\infty}^{\infty} b_z(\Delta\mathbf{r})\, e^{i\mathbf{K}\cdot\Delta\mathbf{r}}\, d^3\Delta\mathbf{r} \tag{2}$$

The integral of eq (2) can be solved for scatterers of particular shapes and sizes. For soft tissues, several researchers have used spherical Gaussian particles to model the scatterers.[6,7] If the scattering particles were modeled as hard particles, the impedance change with the surrounding tissue would be an abrupt discontinuity at the edge of the particle. When the particles are Gaussian scatterers, the impedance change of the particle changes continuously (more slowly) with the surrounding tissue as compared to abruptly for a hard particle. When the scattering particles are assumed to be Gaussian, eq (2) can be evaluated giving the closed-form solution[2]

$$W_{theor}(k) = \left(\frac{a_{eff}^6 nz_{rel}^2}{36\pi^4}\right) e^{-0.827k^2a_{eff}^6} \tag{3}$$

where a_{eff} is the average scatterer radius and nz_{rel}^2 is the average scatterer concentration (number density of scatterers per unit volume times the relative impedance change per particle). The theoretical power spectrum can be normalized to account for the gating function (Hanning window) and beam pattern of the transducer giving[8]

$$W_{theor}(k) = \frac{0.54Lq^2k^4a_{eff}^6 nz_{rel}^2 e^{-0.827k^2a_{eff}^6}}{36\pi^4\left[1+0.16\left(qka_{eff}\right)^2\right]} \tag{4}$$

where L is the gate length and q is the ratio of the transducer radius to the length from the transducer to the ROI.

The measured power spectrum is calculated from a selected ROI in a tissue. The measured power spectrum is the magnitude squared of the Fourier transform of the gated, backscattered RF time signal, $p(t)$, from the ROI

$$W_m(f) = \frac{1}{\sqrt{2\pi}}\left|\int_{t_2}^{t_1} p(t)e^{-i\omega t}\,dt\right|^2 . \tag{5}$$

The effects of the equipment are taken out of the measurement through the substitution method.[9] The substitution method works by comparing the measured power spectrum from an ROI to a reference power spectrum. The reference power spectrum is obtained by reflecting a pulse from a planar reflector through a water path located at the same distance as the ROI from the source. The same equipment and settings used to obtain the measured power spectrum are used to obtain the reference power spectrum. By dividing the measured power spectrum by the reference power spectrum the effects of the equipment and settings are taken out of the measurement.

The measured power spectrum is obtained from an individual ROI that may consist of several A-lines (gated time signals). Averaging the power spectrum from each gated A-line allows for a better statistical description of scattering properties in the ROI. Frequency-dependent attenuation should also be compensated in the measured power spectrum. Including the attenuation-compensation function, $A(f)$, and averaging over the ROI yields for the measured power spectrum[2,3]

$$W_{meas}(f) = \frac{R^2}{4} A(f) \frac{\langle W_m(f) \rangle}{W_{ref}(f)} \tag{6}$$

where R is the reflection coefficient of the planar reflector in water.

The average scatterer parameters, a_{eff} and nz_{rel}^2, can be found by relating the log of the normalized theoretical power spectrum to the log of the measured power spectrum

$$\begin{aligned} 10\log W_{meas}(f) &= 10\log W_{theor}(f) \\ &= 10\log\left[\frac{185Lq^2 f^4 a_{eff}^6 nz_{rel}^2 e^{-13.77 f^2 a_{eff}^6}}{36\pi^4\left[1+2.66\left(qfa_{eff}\right)^2\right]}\right] \end{aligned} \tag{7}$$

where f is in MHz and a_{eff} is in mm. Subtracting the f^4 term from the right hand sides yields

$$10\log\frac{W_{meas}(f)}{f^4} = M\left(a_{eff}\right)f^2 + B\left(a_{eff}, nz_{rel}^2\right). \tag{8}$$

or the equation for a line with $x = f^2$. The slope, M, is a function of a_{eff} and the intercept, B, is a function of a_{eff} and nz_{rel}^2 given by

$$M\left(a_{eff}\right) = -4.34\left[13.77 + 2.66q^2\right]a_{eff}^2 \tag{9}$$

and

$$B\left(a_{eff}, nz_{\text{var}}^2\right) = 10\log\left[185\,Lq^2 a_{eff}^6 n\, z_{\text{var}}^2\right]. \tag{10}$$

By using least squares to fit a line to the measured power spectra, estimates of a_{eff} and nz_{rel}^2 are obtained for each ROI.

As the sound propagates through the tissues, the sound is attenuated and scattered from small microstructures. The attenuation and the scattering are frequency dependent. Furthermore, the initial excitation pulse will have a higher magnitude at the central frequency and lower magnitude at the bandwidth edges (-6dB). As the excitation pulse propagates, typically the higher frequencies are attenuated more rapidly than the lower frequencies. Likewise, different frequencies scatter with different amplitudes based on the size and shape of the scatterers. Inherent in any signal is noise. Those frequency components in the scattered power spectrum that tend to have small magnitude due to the initial excitation bandwidth, the attenuation and the scattering amplitude will also tend to have a smaller signal to noise ratio (SNR). Frequency components with small SNR can lead to greater inaccuracy in the estimates of the scatterer properties.

Weighting different components in the analysis frequency bandwidth according to their expected SNR can reduce the effects of the noise on the estimation of scatterer properties. Extending the work done by Chaturvedi and Insana,[10,11] studies were conducted on improving the accuracy of scatterer estimates in high noise situations.[12] Simulations and phantom experiments were conducted to determine what improvement in scatterer estimations could be made by weighting certain frequency components according to their expected SNR. Figure 1 shows the results of a simulation and phantom experiment for glass bead scatterers (49 ± 2.5 micrometers) embedded in an agar phantom.[13] By weighting the frequency components in the analysis bandwidth according to the excitation bandwidth, the expected attenuation and the expected scattering amplitudes, improvement in scatterer property estimations were made as the backscattered RF signal became more noisy. Essentially the SNR weighting increased the depth to which estimates of scatterer properties could be made. Extending the tissue depth to which scatterer estimates can be made is useful to ultrasound diagnostic capabilities.

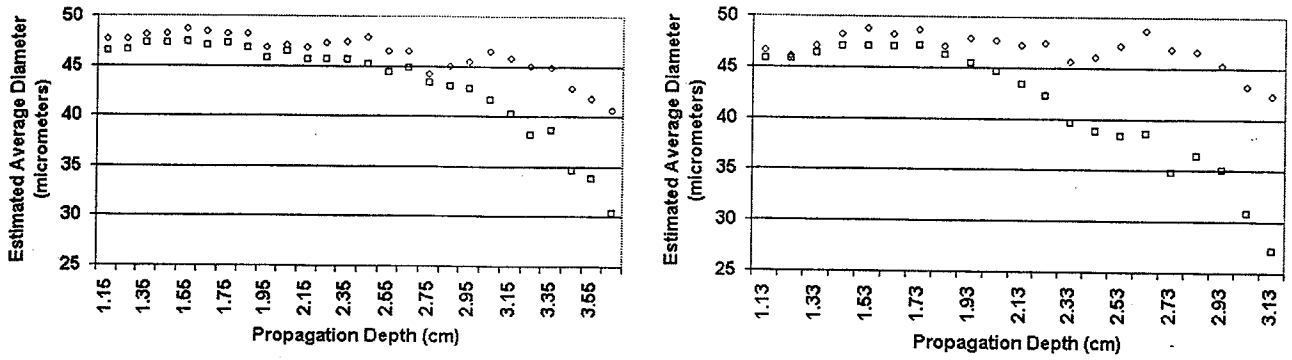

Figure 1 Estimations of glass bead diameters (49 ± 2.5 μm) with propagation depth from simulation (left) and phantom measurements (right); □, without SNR weighting; ◇, with SNR weighting.

III. EXPERIMENT

Eight retired breeder rats (Sprague Dawley, Harlan, Indianapolis) were obtained that had developed spontaneous mammary tumors. The rats were euthanized with CO_2, the area around the tumors was shaved and depilated and the rat was then placed in a holder for ultrasonic scanning. The experimental protocol was approved by the campus Laboratory Animal Care Advisory Committee and satisfied all campus and National Institutes of Health rules for the humane use of laboratory animals. The scans took place in a tank of degassed water heated to 37° C. Scans were obtained by a single-element transducer with central frequency of 8 MHz and a 90% bandwidth. The rats were held upright and the scans were done laterally across the tumor and chest wall. Figure 2 shows a picture of the rat in the holder. A black line was drawn across the tumor and chest to indicate the length and direction of the scan.

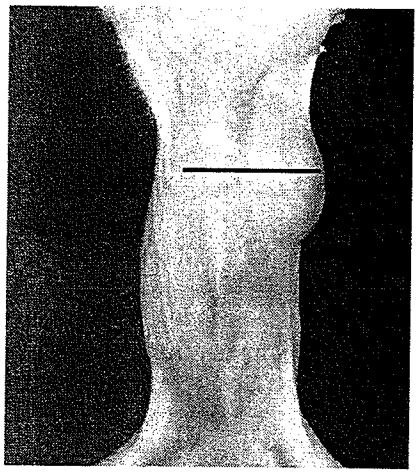

Figure 2 Picture of the rat in holder with mammary tumor on the upper left side of the rat's chest.

Grey-scale B-mode images were constructed from the ultrasonic scans. ROIs were selected from the B-mode images and used to estimate the scattering properties. The ROIs were boxes that were more than 10 wavelengths of the central operating frequency on a side (4 mm). Each ROI had a 75% overlap (sliding Hanning window) with the previous ROI so that pixels of 1mm x 1mm were defined. The backscattered RF time signals were gated from each ROI and the measured power spectra were obtained from an assumed linear attenuation in each rat of 0.7 dB/MHz/cm. After making estimates from the measured power spectra from each ROI, parametric images were constructed for each rat. The parametric images took the two scatterer properties estimated from each ROI and related the estimates to a particular color. The ROI boxes were then superimposed on the conventional gray-scale B-mode images to form two new parametric B-mode images per rat. Figure 3 shows a conventional gray-scale B-mode image of a rat tumor and chest wall. The tumor is located on the

left side of the picture between 0 and 2 cm laterally. Figure 4 shows the parametric B-mode images of the same rat enhanced by the average scatterer size and average scatterer concentration properties, respectively.

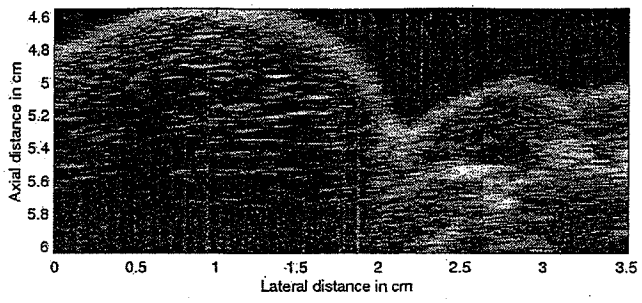

Figure 3 Grey-scale B-mode image of rat tumor (left side of image) and surrounding tissues.

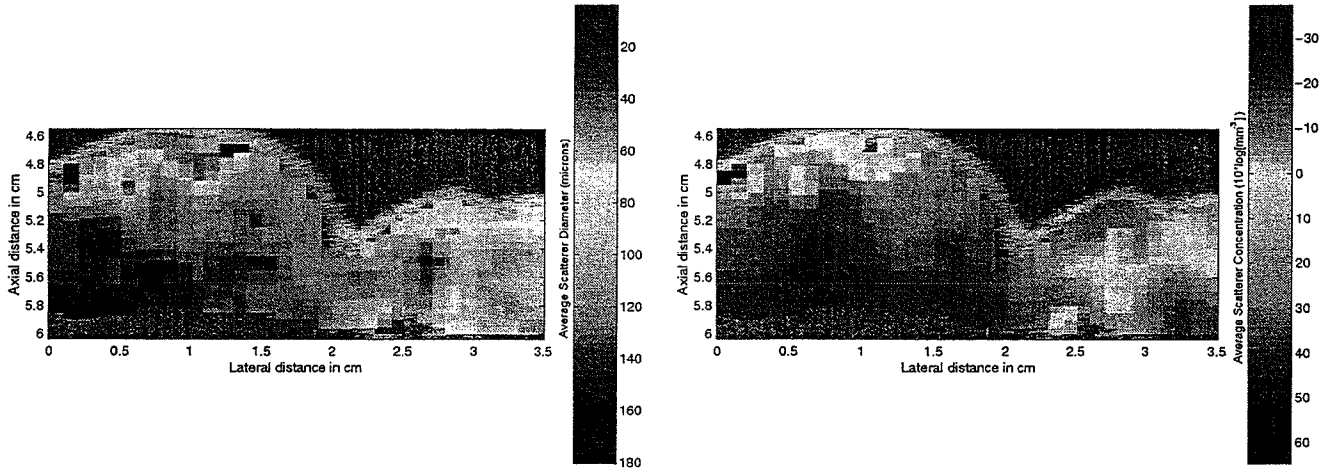

Figure 4 Parametric B-mode images of rats with spontaneous mammary tumors enhanced by the estimated average scatterer diameter (left) and the average scatterer concentration (right) with an assumed attenuation of 0.7 dB/MHz/cm in the tissues.

Several observations were made from the parametric images. First, the scatterer property estimations appeared to have a depth dependence, i.e. the estimations of scatterer sizes increased with the propagation depth in the tissues. The depth dependence was found to be due to attenuation. As the sound propagated through a greater depth, the higher frequency components were attenuated more rapidly than the lower frequency components. If the frequency-dependent losses to the measured power spectrum were undercompensated, the estimations would give scatterer sizes larger than the actual values. If the assumed value for the attenuation was less than the true attenuation in the tissues, then the overestimation of scatterer sizes would be worse with greater depth.

In order to obtain better estimates of the scatterer sizes, the attenuation of the signal was calculated from the backscattered RF signals. The method used to obtain the attenuation of the tissues from the backscatter is outlined in Shung and Thieme.[14] The method assumed that the scattering from regions of shallow propagation depth and greater propagation depth were homogeneous. The only difference between the shallow and deeper regions was the extra attenuation of the signal. By comparing the backscattered returns from different depths the average attenuation was calculated.

The regions outlined by the original parametric images were used to estimate the attenuation in the rats over the frequency ranges used. Columns of 1 mm in width and up to 2 cm in depth were used to calculate the attenuation per column in the rats. By calculating the attenuation per individual column, changes in attenuation from one region to the next could be taken into account. Each column was broken into different sections and the average power spectrum from each section was compared to other sections of the column with different propagation depths. From the comparison, the specific

attenuation for each column was estimated. The attenuation from each column was used to re-estimate the scattering properties associated with the specific attenuation. Figure 5 shows parametric images of a rat with estimates that had been adjusted for the specific column attenuation.

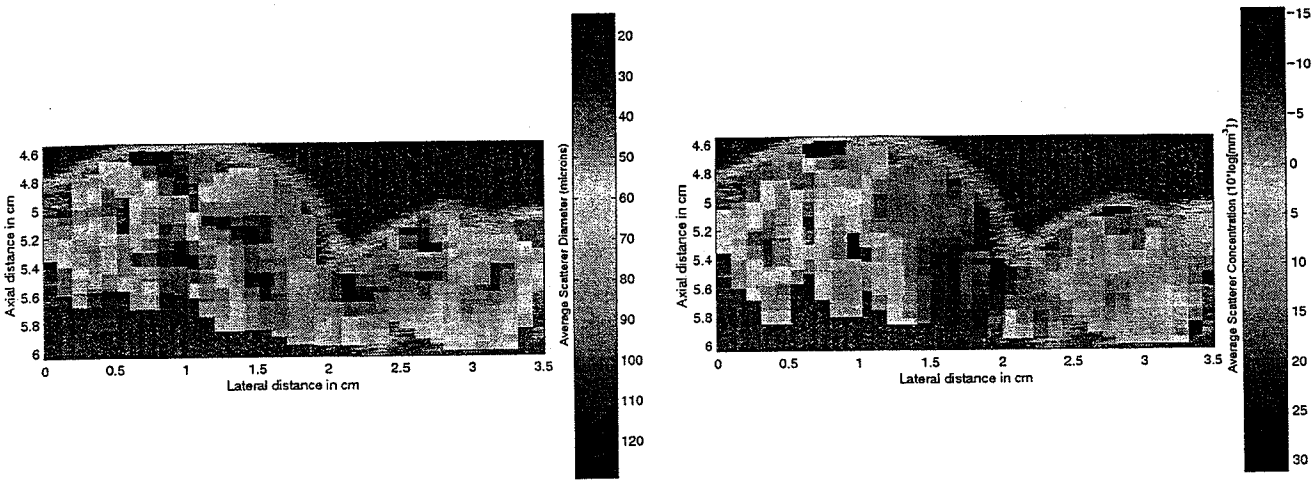

Figure 5 Parametric B-mode images of rats with spontaneous mammary tumors enhanced by the estimated average scatterer diameter (left) and the average scatterer concentration (right) using specific attenuation values obtained from the backscattered RF signals.

A comparison of the parametric images of Figures 4 and 5 show that the depth dependence caused by the attenuation is no longer present. Further examination of the figures shows that there is a correlation between the average scatterer size and the average scatterer concentration. When the average scatterer sizes are larger in one image the corresponding concentration is smaller. If you have smaller scatterers, more scatterers can fit into a unit volume thereby increasing the concentration.

In the parametric images of Figure 5, greater structure is seen in the tissues than in the parametric images of Figure 4. The structure may indicate that there are regions within the tumor that have different microstructure from other regions. The added structure seen in Figure 5 also means that assumption of homogeneous scatterers over a propagation depth is not valid. The estimation of attenuation may be inaccurate because the average scatterer properties changed significantly in certain areas from one ROI to the next.

The effects of the SNR weighting can also be seen from the parametric image of Figure 6. The tumor in the rat of Figure 6 is located on the right side from about 1.3 to 3.5 cm in the lateral direction. The axial length of the tumor in Figure 6 extends almost 2-½ cm in depth. The parametric image created without the SNR weighting (left) began to give increasingly inaccurate estimates at around 6.5 cm in depth until at around 7 to 7.1 cm estimates were unable to be made at all. The parametric image created with the SNR weighting (right) allowed estimates of scatterer properties to be made throughout the total length of the tumor. The diagnostic capability was improved by using the SNR weighting to the analysis bandwidth.

In order to compare scatterer property estimates inside and outside the tumors with minimal effects from the frequency-dependent attenuation losses, only the first half-centimeter in tissue depth was compared. Figure 7 shows the average of the estimations of scatterer diameter and concentration taken inside the tumor and outside the tumor for each of the rats. The average scatterer diameters showed a distinction between tissues inside the tumor and in the surrounding connective tissues. On average there was a 30% difference between diameters estimated in the tumor and in the surrounding tissues. Analysis of the variance of the estimates showed that there was a statistically significant difference ($P < 0.05$) between scatterer diameters inside and outside the tumors ($P = 0.0016$). Similar examination of the average scatterer concentrations showed a statistically significant difference between the tumor and surrounding tissues ($P = 0.0014$).

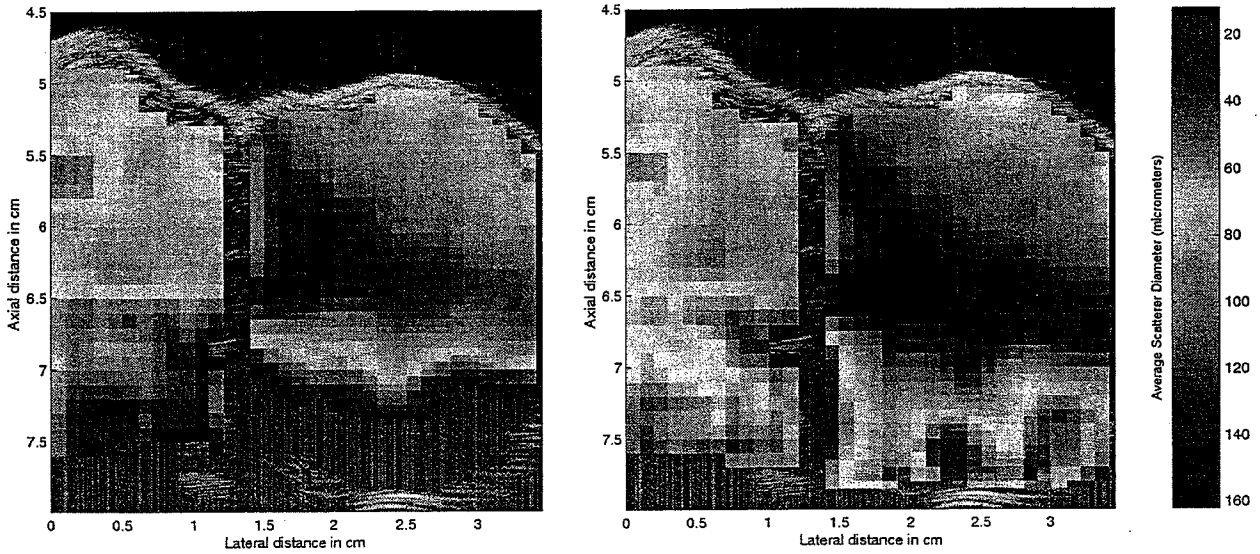

Figure 6 Parametric images of scattering diameters in a rat with mammary tumor without SNR weighting (left) and with SNR weighting.

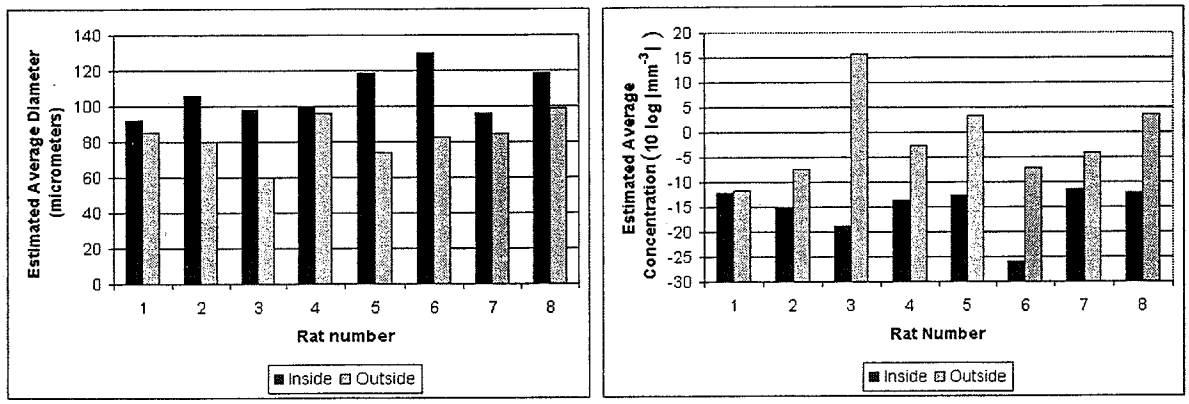

Figure 7 Average estimated scatterer diameters (left) and average estimated scatterer concentrations (right) inside and outside rat tumors.

IV. CONCLUSION

An estimation technique was used to estimate the average scatterer diameter and concentration of tissue microstructure. The estimation technique used least squares to fit a line to the measured power spectrum from ROIs in rats with spontaneous mammary tumors. Parametric images were constructed incorporating the scatterer property estimates.

Techniques were used to improve the accuracy of scatterer property estimates. Weighting frequency components that were expected to have small SNR less than frequency components that were expected to have larger SNR in the analysis bandwidth gave improvement in the accuracy of overall scatterer property estimation. Estimation of the actual attenuation in the tissues was also shown to be important to properly estimating the scatterer properties. Examination of the scatterer property estimates inside and outside the tumors showed that the average scatterer diameter and concentration could be valuable as diagnostic indicators of disease.

ACKNOWLEDGMENTS

Thanks to James P. Blue and Rita J. Miller, DVM, for their technical assistance. This work was supported by NIH Grants CA09067 and CA79179.

REFERENCES

1. J. J. Faran, Jr., "Sound scattering by solid cylinders and spheres," *J. Acoust. Soc. Am.*, **23**, 405-418, 1951.
2. M. F. Insana, R. F. Wagner, D. G. Brown, and T. J. Hall, "Describing small-scale structure in random media using pulse-echo ultrasound," *J. Acoust. Soc. Am.*, **87**, 179-192, 1990.
3. M. F. Insana and T. J. Hall, "Parametric ultrasound imaging from backscatter coefficient measurements: image formation and interpretation," *Ultrason Imaging*, **12**, 245-267, 1990.
4. J. A. Zagzebski, Z. F. Lu, and L. X. Yao, "Quantitative ultrasound imaging: *in vitro* results in normal liver," *Ultrason Imaging*, **15**, 335-351, 1983.
5. E. J. Feleppa, T. Liu, A. Kalisz, M. C. Shao, N. Fleshner, and V. Reuter, "Ultrasonic spectral-parameter imaging of the prostate," *Int. J. Imaging Syst. Technol.*, **8**, 11-25, 1997.
6. D. Nicholas, "Evaluation of backscattering coefficients for excised human tissues: results, interpretation and associated measurements," *Ultrasound Med. Biol.*, **8**, 17-28, 1982.
7. D. K. Nassiri, and C. R. Hill, "The use of angular scattering measurements to estimate structural parameters of human and animal tissues," *J. Acoust. Soc. Am.*, **87**, 179-192, 1990.
8. F. L. Lizzi, M. Astor, T. Liu, C. Deng, D. J. Coleman, and R. H. Silverman, "Ultrasonic spectrum analysis for tissue assays and therapy evaluation," *Int. J. Imaging Syst. Technol.* **8**, 3-10, 1997.
9. F. L. Lizzi, M Greenbaum, E. J. Feleppa, and M. Elbaum, "Theoretical framework for spectrum analysis in ultrasonic characterization," *J. Acoust. Soc. Am.* **73**, 1366-1373, 1983.
10. P. Chaturvedi and M. F. Insana, "Error bounds on ultrasonic scatterer size estimates," *J. Acoust. Soc. Am.*, **100**, 392-399, 1996.
11. P. Chaturvedi and M. F. Insana, "Bayesian and least squares approaches to ultrasonic scatterer size image formation," *IEEE Trans. Ultrason. Ferroelec. Freq. Cont.*, **44**, 152-160, 1997.
12. M. L. Oelze and W. D. O'Brien Jr., "Method of improved scatterer size estimation and application to parametric imaging using ultrasound," *J. Acoust. Soc. Am.* (Submitted 12/20/01).
13. Madsen, E.L., F. Dong, G.R. Frank, B.S. Garra, K.A. Wear, T. Wilson, J.A. Zagzebski, H.L. Miller, K. Shung, S.H. Wang, E.J. Feleppa, T. Liu, W.D. O'Brien, Jr., K.A. Topp, N.T. Sanghvi, A.V. Zaitsev, T.J. Hall, J.B. Fowlkes, O.D. Kripfgans, J.G. Miller, "Interlaboratory comparison of ultrasonic backscatter, attenuation, and speed measurements," *J. Ultrasound Med.*, **18**, pp. 615-631, 1999.
14. K.K. Shung and G. A. Thieme, *Ultrasonic Scattering in Biological Tissues.* CRC Press, Boca Raton, Ann Arbor, London, Tokyo, (1993).